Scheme III

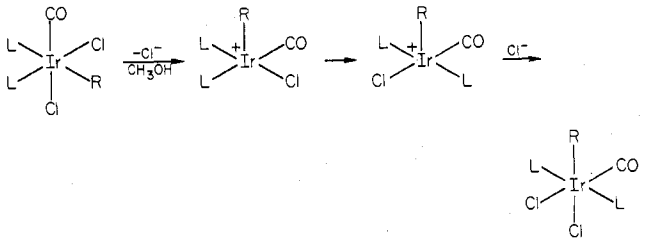

unjustified until the appropriate rate data are available.

The cis → trans isomerizations **1** → **3** are slow relative to the rate of equilibration of **1** and **2** and show clean first-order kinetics. The rates for the ethyl and *n*-propyl complexes **1b** and **1c** are comparable and larger than that of the methyl complex **1a**. In all three cases, isomerization is accelerated by addition of methanol. Thus, for **1b** and **1c**, the half-lives for isomerization are reduced from about 1 week in $CDCl_3$ to 7.7 and 10.4 min, respectively, in 2:1 $CDCl_3/CD_3OD$. For **1c**, the rate of isomerization is increased markedly in the presence of $LiClO_4$ and decreased in the presence of LiCl (see the Experimental Section). These preliminary data are consistent with a mechanism involving rate-determining loss of $Cl^-$ from *cis*-$IrCl_2R(CO)(PMePh_2)_2$ (**1a–c**), rapid rearrangement of the resulting transient five-coordinate alkyliridium(III) cation, and subsequent reentry of $Cl^-$ to give *trans*-$IrCl_2R(CO)(PMePh_2)_2$ (**3a–c**, Scheme III). There is some precedent for cationic species of the type proposed here. Oxidative addition of methyl iodide to $IrCl(CO)(PMe_2Ph)_2$ in benzene is believed to occur via a tight ion pair, $[IrCl(CH_3)(CO)(PMe_2Ph)_2]^+I^-$, but in methanol separation of these ions leads to rapid substitution of chloride by iodide in the iridium(I) complex and thus to a mixture of oxidative addition products.[18] Cationic five-coordinate alkylmetal species are almost certainly formed when rhodium(III) or iridium(III) fluorosulfates or triflates, e.g., $IrClX(CH_3)(CO)(PPh_3)_2$ (X = $SO_3F$, $SO_3CF_3$), are dissolved in polar solvents or when they undergo substitution of X by other ligands,[23–25] and in some cases they can be isolated, e.g., $[RhClR(ttp)]PF_6$ [R = $CH_3$, $C_2H_5$; ttp = $PhP(CH_2CH_2CH_2PPh_2)_2$].[26]

Finally, the fact that despite the smaller size and greater basicity of $PMePh_2$ relative to $PPh_3$ addition of $(CH_3)_2CHCOCl$ to $IrCl(PMePh_2)_3$ still gives exclusively the *n*-alkyl shows the latter to be the thermodynamically favored isomer in these systems, regardless of the nature of the substituents on phosphorus. This assertion is supported by the observation[27] that, although closely related *sec*-alkyl complexes containing dimethylphenylphosphine or trimethylphosphine, *trans*-$IrClR(CO)L_2$ (L = $PMe_2Ph$, $PMe_3$; R = various alkyl groups), can be isolated, they undergo complete isomerization to the corresponding *n*-alkyl in methanol- or water-containing solvents.

**Registry No.** **1a**, 74561-76-5; **1b**, 74524-99-5; **1c**, 74525-00-1; **2b**, 74525-01-2; **2c**, 74525-02-3; **3a**, 19469-17-1; **3b**, 74561-16-3; **3c**, 74561-17-4; $[IrCl(C_8H_{14})_2]_2$, 12246-51-4; $IrCl(PMePh_2)_3$, 63945-96-0; $CH_3COCl$, 75-36-5; $C_2H_5COCl$, 79-03-8; *n*-$C_3H_7COCl$, 141-75-3; 2-methylpropanoyl chloride, 79-30-1.

(23) Strope, D.; Shriver, D. F. *Inorg. Chem.* **1974**, *11*, 2652–2655.
(24) Peterson, J. L.; Nappier, T. E.; Meek, D. W. *J. Am. Chem. Soc.* **1973**, *95*, 8195–8197.
(25) Smith, L. R.; Blake, D. M. *J. Am. Chem. Soc.* **1977**, *99*, 3302–3309.
(26) Tiethof, J. A.; Peterson, J. L.; Meek, D. W. *Inorg. Chem.* **1976**, *15*, 1365–1370.
(27) Bennett, M. A.; Crisp, G. T.; Jeffery, J. C., unpublished work.

Contribution from Lash Miller Chemical Laboratories and Erindale College, University of Toronto, Toronto, Ontario, Canada M5S 1A1

# Optical Spectra of Hafnium, Tungsten, Rhenium, and Ruthenium Atoms and Other Heavy Transition-Metal Atoms and Small Clusters ($Zr_{1,2}$, $Pd_{1,2}$, $Au_{1,2,3}$) in Noble Gas Matrices

WERNER E. KLOTZBÜCHER and GEOFFREY A. OZIN*

*Received November 28, 1979*

Codeposition of transition-metal atoms with weakly interacting, low-temperature matrices has led to the isolation and UV–visible spectroscopic identification of a fairly wide range of atomic, diatomic, and sometimes higher cluster species. In this study, the optical spectra (200–700 nm) have been obtained for Hf, W, Re, and Ru atoms isolated in argon matrices at 10–12 K. The observed lines can be satisfactorily correlated with the reported gas-phase atomic transitions of the respective elements. Blue matrix shifts of roughly 800–2800 $cm^{-1}$ are generally in agreement with the predictions of AMCOR methods. The investigation of these four refractory metals essentially completes a study in which combined resistive-evaporation and matrix-isolation techniques have been utilized to investigate or reexamine the atomic spectra of about 80% of the transition elements. The optical spectra of Zr, Pd, and Au atoms cocondensed with noble gas matrices are reinvestigated under a variety of concentration, deposition, and annealing conditions. By use of relaxed isolation methods, new absorptions are observed which can be associated with $Zr_2$, $Pd_2$, $Au_2$, and $Au_3$. Extended Hückel molecular orbital techniques provide an insight into the electronic and optical properties of some of these heavy-metal molecules. In the case of gold, electronic assignments are discussed in the light of gas-phase optical studies and relativistic molecular quantum mechanical calculations for $Au_2$ and by comparison with the gas- and matrix-phase data for $Ag_2$ and $Ag_3$.

## Introduction

Recently there has been an intensification of interest in the organometallic chemistry of the "electron-rich" refractory elements to the left of the periodic table.[1] Concurrent developments in the metal-vapor chemistry of these heavier elements have also been realized, initially to establish reliable methods for generating and handling the vapors and subsequently to elucidate their potential for the synthesis of novel

* To whom correspondence should be addressed at Lash Miller Chemical Laboratories.

(1) R. R. Schrock, *Acc. Chem. Res.*, **12**, 98 (1979); J. M. Manriquez, D. R. McAlister, R. D. Sanner, and J. E. Bercaw, *J. Am. Chem. Soc.*, **98**, 6733 (1976); K. I. Gell, and J. Schwartz, *J. Chem. Soc., Chem. Commun.*, 244 (1979); E. H. Otto and H. H. Brintzinger, *J. Organomet. Chem.*, **170**, 209 (1979); S. Datta, S. S. Wreford, R. P. Beatty, and T. J. McNeese, *J. Am. Chem. Soc.*, **101**, 1053 (1979), and references cited therein; P. T. Wolczanski and J. Bercaw, *Acc. Chem. Res.*, **13**, 121 (1980).

0020-1669/80/1319-3767$01.00/0 

organometallic compounds. Some representative examples of the latter are illustrated in eq 1–10.

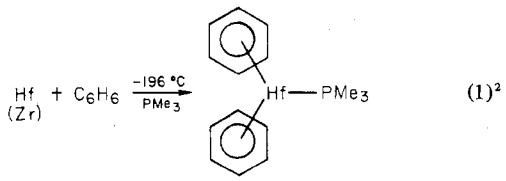


(1)[2]

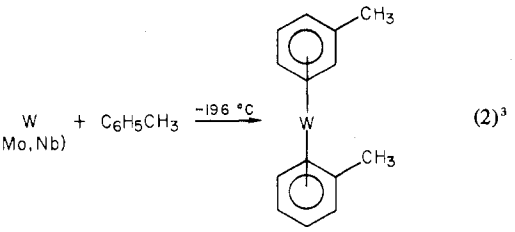


(2)[3]

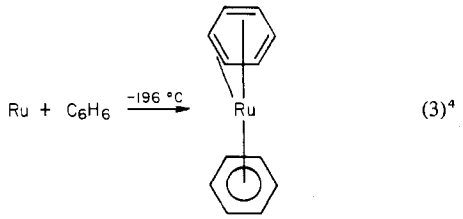


(3)[4]

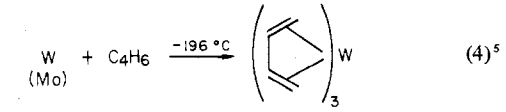


(4)[5]

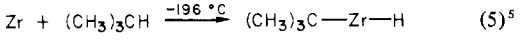


(5)[5]

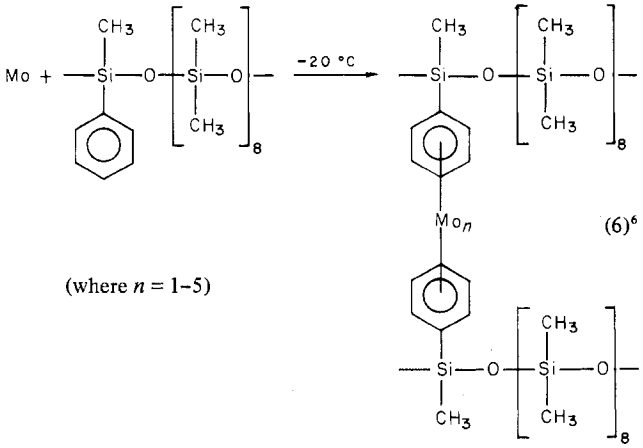


(6)[6]

(where $n$ = 1–5)

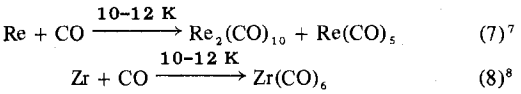


(7)[7]

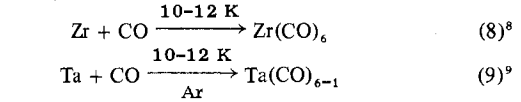


(8)[8]

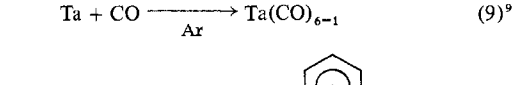


(9)[9]

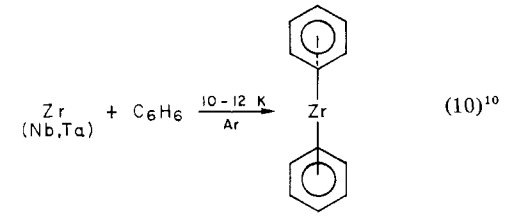


(10)[10]

However, highly refractory metals are notoriously difficult to vaporize, particularly in a highly controlled manner. Moreover, to exactly identify the dominant vapor species can be problematical because of the relatively high impurity levels often prevalent in commercially available, high-melting-point metals as well as the possibility of preferentially volatilizing contaminants in a metal-vapor experiment. Although these complications may only be of minor concern in macroscale metal-vapor experiments involving the refractory metals, they could have disastrous effects at the matrix spectroscopic level of investigation. It is therefore of utmost concern to establish the vaporization and matrix-isolation characteristics of those refractory metals which have, up to the present time, escaped investigation. In this context, we now report the optical spectra of Hf, W, Re, and Ru atoms in argon matrices as well as a preliminary examination of the atomic, diatomic, and higher metal cluster species formed in Zr, Pd, and Au matrix co-condensation reactions.

## Experimental Section

Monoatomic metal vapors were generated by direct resistive heating (ac) of a metal filament or tungsten support suspended between two water-cooled electrodes in furnaces which have been described previously.[11] Zr, Hf, W, Re, and Pd metal were evaporated from thin, ribbon filaments of 99.9+% purity and, in general, 0.010-in. thickness. Gold, available in wire form, was evaporated from a tungsten support. The latter technique was applied to ruthenium powder, but with rather special handling methods which will be described later. The metals were supplied by McKay Inc., New York, and the matrix gases by Matheson of Canada. The rate of metal atom deposition was continuously monitored and controlled with the use of a quartz-crystal microbalance.[12] For the atomic isolation studies, the deposition rate was set such that the probability of a metal atom having another metal atom as a nearest neighbor in the matrix was of the order of $10^{-4}$. Matrix-gas flows, controlled by a calibrated micrometer needle valve and a thermocouple gauge, were maintained at ~2 mmol/h. A Displex closed-cycle helium refrigerator was used to cool a NaCl optical window to 10–12 K, with the temperature being monitored by a Au–0.07 atom % Fe thermocouple embedded in a drilled cavity close to the center of the optical window. UV–visible spectra were recorded on a Unicam SP8000 spectrophotometer in the range 200–700 nm.

## Results

**Hafnium.** The spectra of Hf atoms isolated in cryogenic solids have so far not been reported. The spectrum of HfO in argon and neon matrices has been described by Weltner and McLeod[13] and exhibits a series of absorptions which in Ar occur at 596, 565, 559, 424, 392, 369, and 336 nm.

Hafnium metal can be obtained as wire and foil with a quoted 99+% purity level, which for matrix studies turns out to be insufficient as will be demonstrated shortly. Typical high-purity samples[14] are known to include Cr, Cu, Fe, Ta,

(2) M. L. H. Green and F. G. N. Cloke, *J. Chem. Soc., Chem. Commun.*, 127 (1979).
(3) M. L. H. Green, F. G. N. Cloke, and G. E. Morris, *J. Chem. Soc., Chem. Commun.*, 72 (1978); M. L. H. Green, F. G. N. Cloke, and D. H. Price, *ibid.*, 431 (1978).
(4) P. L. Timms and R. B. King, *J. Chem. Soc., Chem. Commun.*, 989 (1978).
(5) P. S. Skell, E. M. Van Dam, and M. P. Silvon, *J. Am. Chem. Soc.*, **96**, 626 (1974); P. S. Skell, R. J. Remick, and T. A. Asunta, *ibid.*, **101**, 1320 (1979).
(6) C. G. Francis and P. L. Timms (for $n$ = 1), *J. Chem. Soc., Chem. Commun.*, 466 (1977); C. G. Francis, H. Huber, and G. A. Ozin (for $n$ = 2–5), *Inorg. Chem.*, **19**, 219 (1980).
(7) G. A. Ozin and E. P. Kündig, *J. Am. Chem. Soc.*, **96**, 5585 (1974).
(8) W. Klotzbücher and G. A. Ozin, to be submitted for publication.
(9) R. DeKock, *Inorg. Chem.*, **10**, 1205 (1971).
(10) L. Nazar, C. G. Francis, and G. A. Ozin, unpublished work.
(11) W. Klotzbücher, G. A. Ozin, J. G. Norman, Jr., and H. J. Kolari, *Inorg. Chem.*, **16**, 2871 (1977); E. P. Kündig, M. Moskovits, and G. A. Ozin, *J. Mol. Struct.*, **14**, 137 (1972).
(12) M. Moskovits and G. A. Ozin, *J. Appl. Spectrosc. (Engl. Transl.)*, **26**, 481 (1972).
(13) W. Weltner and D. McLeod, *J. Phys. Chem.*, **69**, 3488 (1965).
(14) Goodfellow Metals, Cambridge Science Park, Cambridge, England CB4 4DJ.

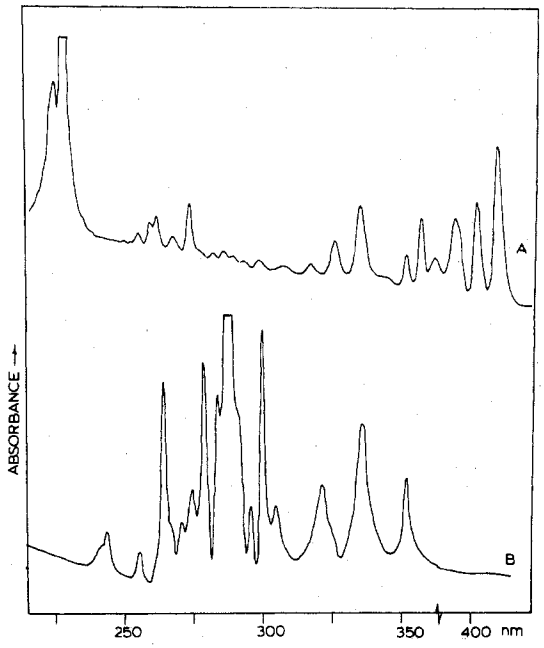


**Figure 1.** (A) Optical spectrum obtained from initial evaporation of a pure hafnium filament, exhibiting a series of absorptions, some of which can be associated with W, Mo, Ta, and Nb. (B) Optical spectrum of hafnium atoms isolated in solid argon at 10–12 K (minor absorptions due to impurities have been subtracted).

Table I. Band Assignments, Matrix Shifts, and Electronic Configurations for Matrix-Isolated Hafnium Atoms (Ground State $5d^26s^2$; $^3F_2$)

| Ar matrix | | gas | shift | confign | | | state | | |
|---|---|---|---|---|---|---|---|---|---|
| λ, nm | $\nu$, $cm^{-1}$ | $\nu$, $cm^{-1}$ | $\Delta\nu$, $cm^{-1}$ | 5d | 6s | 6p | S | L | J |
| | 0 | | | 2 | 2 | 0 | 3 | 3 | 2 |
| 240 | 41 666 | 40 267 | −1399 | | | | | | |
| 244 | 40 983 | 39 704 | −1279 | | | | | | |
| 256 | 39 062 | 38 325 | −737 | | | | | | |
| 265 | 37 735 | 36 949 | −786 | | | | | | |
| 271 | 36 900 | 35 454 | −1446 | | | | | | |
| 275 | 36 363 | 35 284 | −1079 | | | | | | |
| 279 | 35 842 | 34 877 | −965 | | | | | | |
| 284 | 35 211 | 34 596 | −615 | | | | | | |
| 288 | 34 722 | 33 995 | −727 | | | | | | |
| 291 | 34 364 | 33 538 | −826 | | | | | | |
| 296 | 33 783 | 33 122 | −661 | | | | | | |
| 300 | 33 333 | 32 533 | −800 | | | | | | |
| 306 | 32 679 | | | | | | | | |
| 324 | 30 864 | 29 997 | −867 | 2 | 1 | 1 | 3 | 2 | 3 |
| 340 | 29 331 | 28 584 | −747 | 2 | 1 | 1 | 3 | 4 | 3 |
| 360 | 27 777 | 27 150 | −627 | 2 | 1 | 1 | 3 | 3 | 2 |

W, and a rather large amount of Zr. Thorough outgassing at gradually increasing temperatures was found to remove most of the volatile impurities. However, the first few spectra of the metal depositions (as monitored on the quartz-crystal oscillator) are invariably "fake" and display a multitude of lines originating from the contaminants. The majority of these lines can be associated with the refractory metal atoms which are not removed in the original purification of the metal filament and which now are preferentially evaporated (Figure 1A). The "authentic" Hf atom spectrum can eventually be secured following the tedious purification procedure described above. Figure 1B shows a typical subtraction composite trace, as it was impossible to purify the metal completely. Correlations with the gas-phase data[15] are satisfactory and are listed in Table I. A general blue shift of some 800–1400 $cm^{-1}$ for all of the Hf/Ar absorptions from the Hf gas-phase positions is in line with shifts previously observed for Ti[21,31] and Zr[18] atoms.

Table II. Band Assignments, Matrix Shifts, and Electronic Configurations for Matrix-Isolated Tungsten Atoms (Ground State $5d^46s^2$; $^5D_0$)

| Ar matrix | | gas | shift | confign | | | state | | |
|---|---|---|---|---|---|---|---|---|---|
| λ, nm | $\nu$, $cm^{-1}$ | $\nu$, $cm^{-1}$ | $\Delta\nu$, $cm^{-1}$ | 5d | 6s | 6p | S | L | J |
| | 0 | | | 4 | 2 | 0 | 5 | 2 | 0 |
| 196 | 51 020 | | | | | | | | |
| 199 | 50 251 | | | | | | | | |
| 203 | 49 261 | | | | | | | | |
| 208 | 48 076 | | | | | | | | |
| 213 | 46 948 | 43 893 | −3055 | | | | | | |
| 216 | 46 296 | | | | | | | | |
| 219 | 45 662 | 43 217 | −2445 | | | | | | |
| 224 | 44 642 | 42 262 | −2380 | | | | | | |
| 227 | 44 052 | | | | | | | | |
| 233.5 | 42 826 | | | | | | | | |
| 237 | 42 194 | | | | | | | | |
| 240 | 41 666 | | | | | | | | |
| 244 | 40 983 | 40 771 | −212 | | | | | | |
| 247.5 | 40 404 | | | | | | | | |
| 250 | 40 000 | 39 183 | −817 | | | | | | |
| 254 | 39 370 | 38 356 | −1014 | | | | | | |
| 263 | 38 022 | | | | | | | | |
| 272 | 36 764 | 36 180 | −574 | | | | | | |
| 276 | 36 231 | | | | | | | | |
| 281 | 35 587 | 34 719 | −868 | | | | | | |
| 284 | 35 211 | 34 342 | −869 | | | | | | |
| 300 | 33 333 | | | | | | | | |
| 310 | 32 258 | 31 323 | −935 | | | | | | |
| 345 | 28 985 | 28 199 | −786 | 4 | 1 | 1 | 5 | 1 | 1 |
| 375 | 26 666 | 25 984 | −682 | 4 | 1 | 1 | 5 | 3 | 1 |
| 438 | 22 831 | | | | | | | | |
| 453 | 22 075 | 21 454 | −621 | 4 | 1 | 1 | 7 | 2 | 1 |
| 464 | 21 551 | | | | | | | | |
| 482 | 20 746 | 20 064 | −682 | 4 | 1 | 1 | 7 | 3 | 1 |

Reproducible results can be obtained when Hf is evaporated from a previously outgassed tungsten support. The metals do not seem to alloy. For example, completion of Hf evaporation during an experiment can easily be detected by the appearance of W atomic resonance absorptions. However, it is recommended that a considerable proportion of the metal should be preevaporated before commencing a matrix-isolation experiment with commercially available hafnium.

**Tungsten.** Tungsten vapor was generated from either a center-thinned filament (99.95%, 0.010 in.) or rod (0.025-in. diameter) of the metal. The single most important impurity in the metal is listed as molybdenum (150 ppm).[14]

Because of the difficulty of vaporizing tungsten, which requires a vapor pressure of $10^{-4}$ torr at 3000 K, it is not too surprising that little has been said about matrix-isolated tungsten atoms. Schoch and Kay[16] reported the evaporation of tungsten atoms by a triode sputtering source into argon and xenon. Their matrix spectra exhibited broad, overlapping lines, only some of which could be correlated with the stronger absorptions reported for gas-phase tungsten.[15]

A typical spectrum obtained in this study after resistive evaporation of tungsten and trapping in argon is displayed in Figure 2, and the data are summarized in Table II. A number of sharp spectral absorptions between 200 and 275 nm can be satisfactorily correlated with the known gas-phase spectra,[15] with an average matrix-induced blue shift of roughly 800 $cm^{-1}$.

A number of weaker absorptions in both the high- and low-energy regions of the spectrum could not be attributed to any particular gas-phase absorption. The origin of these additional lines is not clear at present. Consistent appearance

(15) D. H. W. Carstens, H. Brashear, D. R. Eslinger, and D. M. Gruen, *Appl. Spectrosc.*, **26**, 184 (1972).

(16) F. Schock and E. Kay, *J. Chem. Phys.*, **59**, 718 (1973).

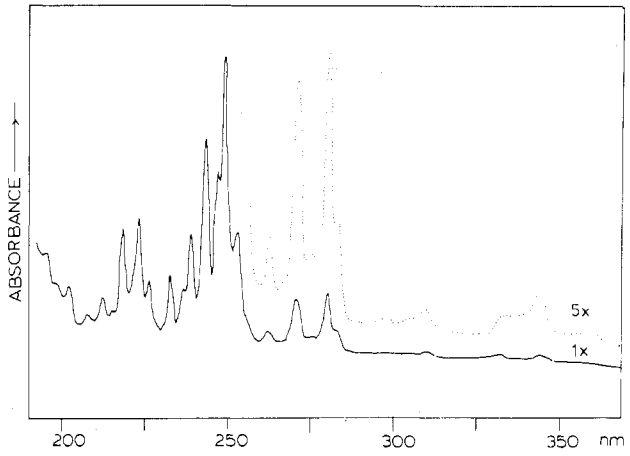


**Figure 2.** Optical spectrum of tungsten atoms isolated in solid argon at 10–12 K (with expansion of the weak, low-energy lines).

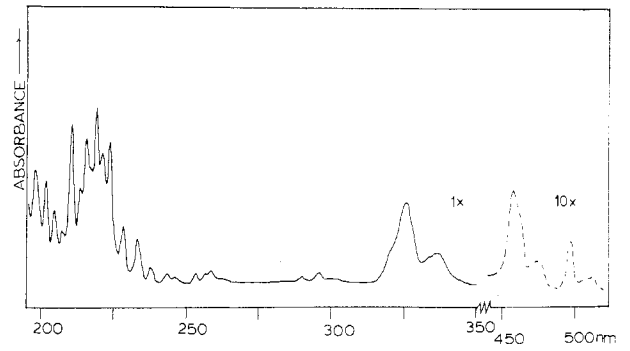


**Figure 3.** Optical spectrum of rhenium atoms isolated in solid argon at 10–12 K.

and constant relationship to the stronger features seem to exclude the possibility of ascribing these absorptions to impurity complexes or small metal clusters. One might speculate that for matrix-entrapped, *third-row metals* there is a greater likelihood of experiencing a more pronounced breakdown of the atomic transition selection rules which could be manifested in the appearance of weak absorptions that normally correspond to forbidden transitions.

**Rhenium.** Rhenium is one of the rarest metals in the earth's crust, having a natural abundance of only some $10^{-9}$%, and was the last of the stable elements to be discovered some 50 years ago. Its melting point is surpassed only by that of tungsten. All of the comments made on the idiosyncracies of tungsten evaporation apply equally well to rhenium, although with due care no real evaporation problems were encountered from a center-thinned filament (99.9+%, 0.010 in.) at approximately 3100 K. Considering the high temperature required in these experiments, it is again not surprising that no reports on the isolation of Re atoms in matrices have so far appeared in the literature, although Re/CO matrix reactions at 10–12 K have been shown to yield $Re(CO)_5$ and $Re_2(CO)_{10}$.[7]

The optical spectrum resulting from the cocondensation of rhenium vapor with argon at approximately 12–15 K is displayed in Figure 3, and the data are summarized and correlated with gas-phase data in Table III. (The slightly higher matrix deposition temperature was caused by the effects of radiation heating of the optical window from the rhenium filament.) The multitude of lines with comparable intensities in the high-energy region allows only tentative correlations with the gas-phase data.[15] However, a regular, blue matrix shift of some 2000 $cm^{-1}$ is consistent with the trend observed for other third-row metals.[17]

Table III. Band Assignments, Matrix Shifts, and Electronic Configurations for Matrix-Isolated Rhenium Atoms (Ground State $5d^56s^2$; $^6S_{5/2}$)

| Ar matrix | | gas | shift | confign | | | state | | |
|---|---|---|---|---|---|---|---|---|---|
| λ, nm | $\nu$, $cm^{-1}$ | $\nu$, $cm^{-1}$ | $\Delta\nu$, $cm^{-1}$ | 5d | 6s | 6p | S | L | J |
| | 0 | | | 5 | 2 | 0 | 6 | 0 | $^5/_2$ |
| 198 | 50 505 | 47 932 | −2573 | 6 | 0 | 1 | 6 | 3 | $^7/_2$ |
| 201.5 | 49 627 | 47 669 | −1958 | | | | | | |
| 204.5 | 48 899 | 46 112 | −2787 | | | | | | |
| 207 | 48 309 | 45 937 | −2372 | | | | | | |
| 210.5 | 47 505 | 44 148 | −3357 | | | | | | |
| 213.5 | 46 838 | 43 950 | −2888 | | | | | | |
| 215.5 | 46 403 | 43 818 | −2588 | 5 | 1 | 1 | 6 | 1 | $^3/_2$ |
| 217 | 46 082 | 43 702 | −2380 | | | | | | |
| 219 | 45 662 | 43 569 | −2093 | 5 | 1 | 1 | 6 | 1 | $^5/_2$ |
| 221 | 45 248 | 42 254 | −2994 | 5 | 1 | 1 | 4 | 2 | $^3/_2$ |
| 223.5 | 44 792 | 41 313 | −3429 | 5 | 1 | 1 | 6 | 2 | $^5/_2$ |
| 228 | 43 859 | 41 164 | −2695 | 5 | 1 | 1 | 6 | 2 | $^7/_2$ |
| 233 | 42 918 | 40 809 | −2109 | 5 | 1 | 1 | 6 | 1 | $^3/_2$ |
| 237.5 | 42 105 | 39 845 | −2260 | 5 | 1 | 1 | 6 | 1 | $^7/_2$ |
| 243 | 41 152 | 39 670 | −1482 | | | | | | |
| 246 | 40 650 | 39 065 | −1585 | 4 | 2 | 1 | 6 | 3 | $^5/_2$ |
| 253 | 39 525 | 37 916 | −1609 | 5 | 1 | 1 | 4 | 1 | $^3/_2$ |
| 256.5 | 38 986 | 37 698 | −1288 | | | | | | |
| 258.5 | 38 684 | 37 381 | −1303 | 5 | 2 | 1 | 6 | 4 | $^5/_2$ |
| 276 | 36 231 | 34 520 | −1711 | 4 | 2 | 1 | 6 | 2 | $^7/_2$ |
| 289.5 | 34 542 | 33 589 | −953 | 4 | 2 | 1 | 6 | 1 | $^3/_2$ |
| 295.5 | 33 840 | 33 409 | −431 | 4 | 2 | 1 | 6 | 2 | $^5/_2$ |
| 301.5 | 33 167 | 32 592 | −575 | 4 | 2 | 1 | 6 | 2 | $^3/_2$ |
| 320 | 31 250 | 28 962 | −2288 | 5 | 1 | 1 | 6 | 1 | $^3/_2$ |
| 326 | 30 674 | 28 890 | −1784 | 5 | 1 | 1 | 6 | 1 | $^7/_2$ |
| 337 | 29 673 | 28 854 | −819 | 5 | 1 | 1 | 6 | 1 | $^5/_2$ |
| 458 | 21 834 | 20 448 | −1386 | 5 | 1 | 1 | 8 | 1 | $^7/_2$ |
| 497 | 20 120 | 18 950 | −1170 | 5 | 1 | 1 | 8 | 1 | $^5/_2$ |

**Ruthenium.** Ruthenium proved to be one of the most difficult metals to evaporate as a monoatomic vapor. The metal is available only in powder form of 99.9+% purity, with the major impurity being osmium.[14] It was found that near the expected evaporation temperature of approximately 2400 K the metal rapidly alloys with the tantalum Knudsen cell. Although the cell retained its integrity even at higher temperatures, it broke down mechanically on slow cooling to room temperature.

In another attempt, ruthenium in a separately outgassed graphite Knudsen cell led to a brittle, metal–carbon combination at elevated temperatures but again with no sign of evaporation. Attaching the powder with wax or oil to a tungsten boat was also unsuccessful. The apparent carbide formation led to burn-out of the combination before evaporation.

Fortunately, it had recently been demonstrated in a macroscale metal vapor synthesis of $(\eta^4\text{-}C_6H_6)(\eta^6\text{-}C_6H_6)Ru$[4] that it is possible to evaporate ruthenium powder by attaching it to a carrier material in an epoxy-based heating process. This concept was utilized as the basis for our Ru evaporation process. By mixing ruthenium powder with the epoxy, but without the hardener, followed by smearing the resulting glue onto a tungsten boat, it was possible to gain both mechanical stability and, after extensive and slow outgassing, a stable Ru-vapor deposition at low rates. In this way, the spectrum of matrix-isolated ruthenium atoms was observed for the first time, a typical spectrum being shown in Figure 4. It should be noted that the aforementioned outgassing process is a rather sensitive undertaking, since at higher evaporation temperatures the rate of alloy formation becomes so rapid that only preferential evaporation of tungsten from the ensuing Ru/W composition can be observed. The matrix atomic Ru spectrum

(17) Neither narrow-band 325-nm nor broad-band irradiation from a 450-W xenon lamp resulted in changes in the Re atom spectrum.

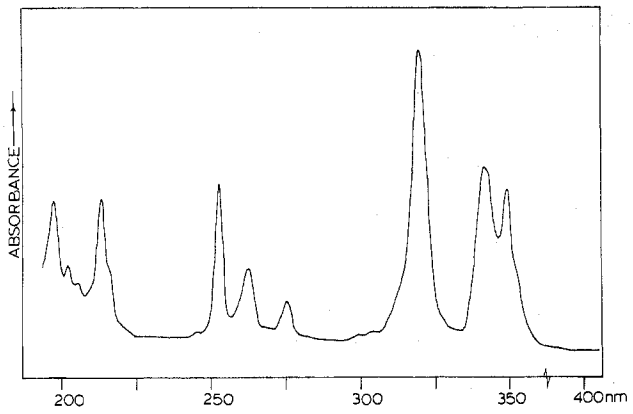


**Figure 4.** Optical spectrum of ruthenium atoms isolated in solid argon at 10–12 K.

Table IV. Band Assignments, Matrix Shifts, and Electronic Configurations for Ruthenium Atoms (Ground State $4d^75s^1$; $^5F_5$) Isolated in Argon Matrices

| Ar matrix | | gas | shift | confign | | | state | | |
|---|---|---|---|---|---|---|---|---|---|
| λ, nm | ν, cm$^{-1}$ | ν, cm$^{-1}$ | Δν, cm$^{-1}$ | 4d | 5s | 5p | S | L | J |
| | 0 | | | 7 | 1 | 0 | 5 | 3 | 5 |
| 197 | 50 761 | 44 322 | −6439 | 6 | 1 | 1 | 5 | 3 | 5 |
| 197 | 50 761 | 44 243 | −6578 | 6 | 1 | 1 | 5 | 2 | 4 |
| 214 | 46 728 | 43 999 | −2729 | | | | | | |
| 252.5 | 39 603 | 36 543 | −3060 | 7 | 0 | 1 | 5 | 2 | 4 |
| 262 | 38 167 | 34 773 | −3394 | 6 | 1 | 1 | 5 | 3 | 5 |
| 275 | 36 363 | 33 447 | −2916 | 6 | 1 | 1 | 5 | 2 | 4 |
| 314 | 31 847 | 29 161 | −2686 | 6 | 1 | 1 | 7 | 3 | 6 |
| 319.5 | 31 298 | 28 572 | −2726 | 7 | 0 | 1 | 5 | 4 | 6 |
| 341.5 | 29 282 | 26 826 | −2466 | 7 | 0 | 1 | 5 | 3 | 5 |
| 349 | 28 653 | 26 313 | −2340 | 7 | 0 | 1 | 5 | 2 | 4 |

can be reasonably well correlated with the gas-phase spectrum,[15] noting a matrix-induced shift of approximately 2800 cm$^{-1}$, with greater shifts at higher transition energies (Table IV).

Finally, it is worth noting that 345-nm continuous irradiation into the $4d^75s^1 \rightarrow 4d^75p^1$ Ru atomic absorption resulted only in slow loss of Ru atom intensity. In neither these experiments nor those involving broad-band irradiations could the growth of any new $Ru_n$ cluster lines be observed. Similarly, in thermal annealing experiments, loss of atom intensity was again observed, without however accompanying spectral changes indicating the formation of small $Ru_n$ clusters.

**Osmium.** All attempts to evaporate osmium powder from tantalum or graphite Knudsen cells failed, probably for the reasons outlined in the ruthenium study, as did all attempts to evaporate the metal from a tungsten boat. Interestingly, even the epoxy method resulted only in either a band at 400 nm, most probably associated with an unidentified W/Os bimetallic cluster, or the preferential evaporation of tungsten as seen by its characteristic matrix atomic spectrum. Visual inspection showed the osmium to be still present on the carrier. From gas-phase data,[15] a multitude of absorptions between 200 and 400 nm are to be expected upon successful isolation of atomic Os.

**Zirconium.** During the completion of this study, Bates and Gruen[18] published the first account of the absorption spectra of Zr atoms isolated in inert-gas matrices. They utilized a hollow-cathode vaporization source which, apart from producing the desired atomic Zr, also resulted in the generation and trapping of small amounts of impurities as well as some ZrO. Our data differ sufficiently from those of Bates and Gruen[18] to warrant further discussion.

(18) J. K. Bates and D. M. Gruen, *High Temp. Sci.*, **10**, 27 (1978).

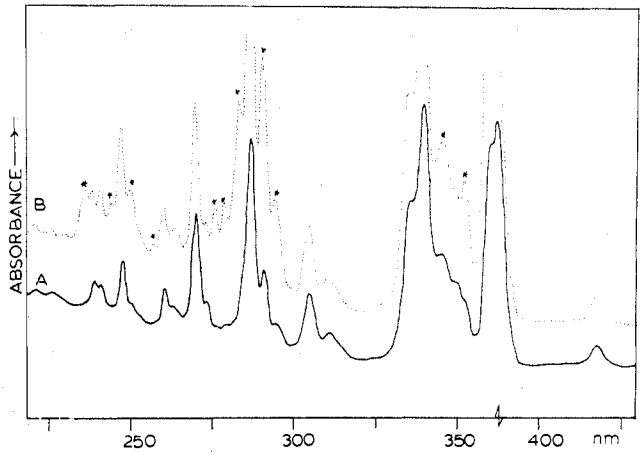


**Figure 5.** (A) Optical spectrum of zirconium atoms isolated in solid argon at 10–12 K. (B) Spectrum obtained after insufficient outgassing and preevaporation, showing Mo and W impurities marked by an asterisk.

Table V. Band Assignments, Matrix Shifts, and Electronic Configurations for Matrix-Isolated Zirconium Atoms (Ground State $4d^25s^2$; $^3F_2$)

| Ar matrix | | gas | shift | confign | | | state | | |
|---|---|---|---|---|---|---|---|---|---|
| λ, nm | ν, cm$^{-1}$ | ν, cm$^{-1}$ | Δν, cm$^{-1}$ | 4d | 5s | 5p | S | L | J |
| | 0 | | | 2 | 2 | 0 | 3 | 3 | 2 |
| 210 | 47 619 | | | | | | | | |
| 221 | 45 248 | | | | | | | | |
| 226 | 44 247 | | | | | | | | |
| 239.5 | 41 753 | | | | | | | | |
| 241.5 | 41 407 | | | | | | | | |
| 248 | 40 322 | | | | | | | | |
| 261 | 38 314 | 36 942 | −1372 | 3 | 0 | 1 | 3 | 4 | 3 |
| 264 | 37 878 | | | | | | | | |
| 270.5 | 36 968 | 35 806 | −1162 | 2 | 1 | 1 | 3 | 3 | 2 |
| 274 | 36 496 | 35 515 | −981 | 2 | 1 | 1 | 3 | 3 | 3 |
| 287.5 | 34 782 | 33 764 | −1018 | 2 | 1 | 1 | 3 | 2 | 1 |
| 291.5 | 34 305 | 33 487 | −818 | 2 | 1 | 1 | 3 | 2 | 2 |
| 295 | 33 898 | | | | | | | | |
| 305 | 32 786 | 31 327 | −1459 | 3 | 0 | 1 | 3 | 4 | 3 |
| 310.5 | 32 206 | | | | | | | | |
| 336 | 29 761 | 28 801 | −960 | 2 | 1 | 1 | 3 | 2 | 1 |
| 340.5 | 29 368 | 28 404 | −964 | 2 | 1 | 1 | 3 | 4 | 3 |
| 346 | 28 901 | 28 157 | −747 | 2 | 1 | 1 | 3 | 3 | 3 |
| 350 | 28 571 | 27 876 | −695 | 2 | 1 | 1 | 3 | 3 | 2 |
| 372 | 26 881 | 26 154 | −727 | 2 | 1 | 1 | 3 | 2 | 1 |
| 376 | 26 595 | 26 062 | −533 | 2 | 1 | 1 | 3 | 3 | 2 |
| 376 | 26 595 | 25 730 | −865 | 3 | 0 | 1 | 3 | 4 | 3 |
| 435 | 22 988 | 21 849 | −1139 | 2 | 1 | 1 | 3 | 4 | 3 |

Zirconium metal can be obtained as both wire and foil with 99.8+% purity. From the results of the present study it seems evident that this level of contamination if sufficiently high to cause serious problems in Zr vapor matrix-isolation experiments. The metal as supplied is known to contain large amounts of O (1000 ppm), Cr (100 ppm), Fe (600 ppm), Hf (65 ppm), Sn (100 ppm), and C (120 ppm), to name only the most common impurities.[15] Thorough outgassing at gradually increasing temperatures removes most of the gaseous and most volatile components. By monitoring of the deposition spectroscopically, one or two "fake" depositions are observed as described earlier. The first "true" Zr vapor deposition, in general, still reveals some extraneous absorption lines, which seem to belong to molybdenum and tungsten (Figure 5A).

Evaporation was found to be most conveniently achieved by using zirconium foil wrapped around a tungsten support. Our best spectroscopic results were obtained when the sample was used only after a substantial amount of metal had been preevaporated. Under these circumstances the spectrum for zirconium atoms isolated in argon matrices at 10–12 K was

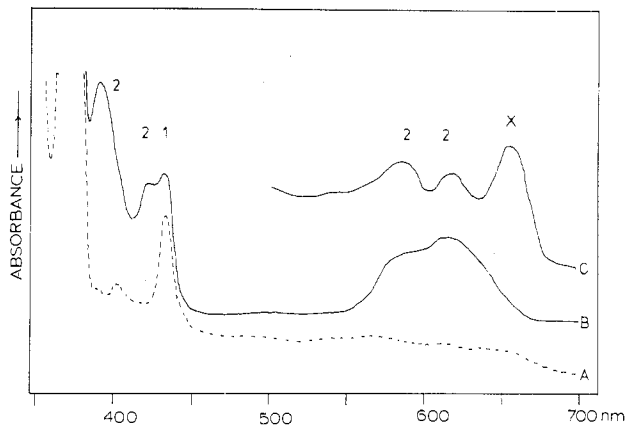


**Figure 6.** Optical spectrum of zirconium atoms cocondensed with argon at (A) low and (B) higher concentrations, showing the growth of $Zr_2$ absorptions and (C) the appearance of a new line upon cocondensation at even higher metal deposition rate (see text).

**Table VI.** The UV-Visible Spectra of $Zr_2$, $Pd_2$, $Au_2$, and $Au_3$ in a Solid Argon Matrix at 10-12 K

| metal | $\lambda_{Ar}$, nm | $\nu_{Ar}$, $cm^{-1}$ | assignt |
|---|---|---|---|
| Zr | 390 | 25 641 | $Zr_2$ |
| | 422 | 23 696 | $Zr_2$ |
| | 585 | 17 094 | $Zr_2$ |
| | 615 | 16 260 | $Zr_2$ |
| Pd | 265 | 37 735 | $Pd_2$ |
| Au | 198 | 50 505 | $Au_2$ |
| | 208 | 48 076 | $Au_2$ |
| | 317 | 31 545 | $Au_2$ |
| | 365 | 27 397 | $Au_2$ |
| | 292 | 34 246 | $Au_3$ |
| | 471 | 21 231 | $Au_3$ |

obtained and is shown in Figure 5B. As expected, a multitude of overlapping bands is observed in the region 250–400 nm, most of which can be correlated with those of the stronger absorptions of gaseous Zr,[15] if one invokes a blue matrix shift of some 800 $cm^{-1}$ (Table V).

As mentioned earlier, Bates and Gruen[18] recently published the absorption spectra of Zr atoms and ZrN isolated in rare-gas matrices. Two different sputtering sources were employed, an ion gun and a hollow cathode discharge. The spectra for zirconium atoms produced by these methods differ considerably. However, upon annealing, the spectra convert to the spectrum produced by the ion-gun technique.

The spectroscopic data for Zr atoms produced by resistive heating in this study are in close agreement (in the region 250–400 nm) with Gruen's[18] spectra of Zr atoms produced by ion-gun sputtering. However, the sharp Zr and ZrO[19] lines mentioned in Gruen's work in the low-energy region between 500 and 700 nm were not observed. In our investigations this region is virtually absorption free (Figure 6A). The ion-gun vaporization method is known to produce not only atoms but also dimeric and higher cluster species due to the kinetic mobility of the highly energized atoms on the matrix surface during deposition.[18] Together with the known impurity content of zirconium metal,[15] this might account for the difference in results. It should be noted, however, that a minor discrepancy exists in the assignment of some of the absorptions of matrix-isolated Zr atoms. Gruen's assignments would result in an average spectral shift of 1500 $cm^{-1}$ from the gas-phase lines, while the AMCOR preferred in this study leads to a shift of the order of 800 $cm^{-1}$ (Table V).

(19) Weltner and McLeod[13] reported that the spectrum of ZrO in argon shows bands at 663, 602, 530, and 368 nm.

Table VII

A. Optimized Zr and Pd Parameters Used in Extended Hückel Calculations of $Zr_2$ and $Pd_2$

| metal $r_e$, Å | orbital | orbital coeff | $H_{ii}$, eV |
|---|---|---|---|
| Zr, 2.50 | 4p | 3.367 | −34.50 |
| | 4d | 3.248 | −5.00 |
| | 5s | 1.302 | −6.00 |
| | 5p | 0.990 | −3.75 |
| Pd, 2.70 | 4p | 4.500 | −63.99 |
| | 4d | 3.646 | −8.70 |
| | 5s | 1.583 | −7.00 |
| | 5p | 1.354 | −3.50 |

B. Correlation between Calculated and Observed Electronic Transitions of $Zr_2$ and $Pd_2$

| | | transition, $cm^{-1}$ | |
|---|---|---|---|
| molecule | assignt | calcd (EHMO) | obsd (argon) |
| $Zr_2$ | $1\sigma_g \rightarrow 2\sigma_u$ | 16 030 | 16 260, 17 094 |
| | $1\sigma_g \rightarrow 2\pi_u$ | 21 101 | 23 696 |
| | $1\pi_u \rightarrow 3\sigma_g$ | 23 297 | 25 641 |
| $Pd_2$ | $1\sigma_g \rightarrow 2\pi_u$ | 38 146 | 37 735 |

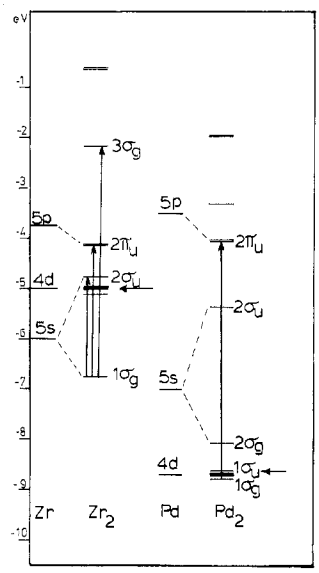


**Figure 7.** EHMO energy level schemes calculated for $Zr_2$ and $Pd_2$ at internuclear distances of 2.50 and 2.70 Å, respectively.

Cocondensation of Zr vapor with argon at Zr/Ar ratios higher than $1/10^4$ results in the appearance of four *new* absorptions at 390, 422, 585, and 615 nm, which, from concentration studies, can be associated with a single zirconium cluster (Figure 6, Table VI). Under the conditions chosen, clusters higher than binuclears would not be expected to form. Thus it seems reasonable to assign these new lines to the $Zr_2$ species. However, it should be emphasized that our concentration studies were limited, as zirconium alloyed rapidly with the W support at the higher temperatures (required for faster Zr deposition rates), as seen by the appearance of an extraneous line at about 652 nm, most probably associated with a W/Zr cluster species (Figure 6C).

Apart from this study, no experimental data have been published on $Zr_2$, although it is interesting to note that Gingerich[20] recently predicted a $Zr_2$ bond dissociation energy between 70 and 80 kcal/mol.

We have previously demonstrated[11,21] that extended Hückel calculations can provide a useful first insight into the molecular

(20) A. R. Miedema and K. A. Gingerich, *J. Phys. B*, **12**, 2081 (1979).
(21) R. Busby, W. Klotzbücher, and G. A. Ozin, *J. Am. Chem. Soc.*, **98**, 4013 (1976); G. A. Ozin and W. E. Klotzbücher, *Inorg. Chem.*, **18**, 2101 (1979).

Table VIII. Band Assignments and Matrix Shifts for Palladium (Ground State $4d^{10}; {}^1S_0$)

| upper state | λ, nm | ν, cm$^{-1}$ | λ, nm | ν, cm$^{-1}$ | Δν, cm$^{-1}$ | λ, nm | ν, cm$^{-1}$ | Δν, cm$^{-1}$ | λ, nm | ν, cm$^{-1}$ | Δν, cm$^{-1}$ |
|---|---|---|---|---|---|---|---|---|---|---|---|
| | Gas | | Argon[a] | | | Krypton[a] | | | Xenon | | |
| $^1P_1$ | 244 | 40 839 | B 220 | 45 454 | −4615 | B 214 | 46 728 | −5889 | 216 | 46 296 | −5457 |
| | | | A 227 | | | A 218 | 45 871 | −5032 | | | |
| $^3D_1$ | 247 | 40 369 | B 236 | 42 372 | −2003 | B 223 | 44 843 | −4474 | 230 | 43 478 | −3109 |
| | | | A 245 | | | A 238 | 42 016 | −1647 | | | |
| $^3P_1$ | 276 | 36 181 | B 248 | 40 322 | −4141 | B 245 | 40 816 | −4635 | 235 | 42 553 | −6372 |
| | | | A 253 | | | A 253 | 39 528 | −3344 | | | |
| | | | | | | Propane | | | Hexane | | |
| | 244 | 40 839 | | | | 228 | 43 859 | −3020 | 232 | 43 103 | −2264 |
| | 247 | 40 369 | | | | 247 | 40 485 | −116 | 252 | 39 682 | +687 |
| | 276 | 36 181 | | | | 261 | 38 314 | −2133 | 268 | 37 313 | −1132 |

[a] A and B represent different matrix trapping sites for atomic Pd.

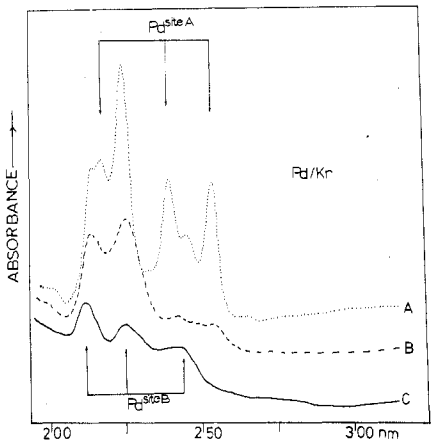


**Figure 8.** Optical spectrum of palladium atoms isolated in solid krypton (A) after deposition at 10–12 K, (B) after warm-up to 20 K, and (C) after annealing to 25 K.

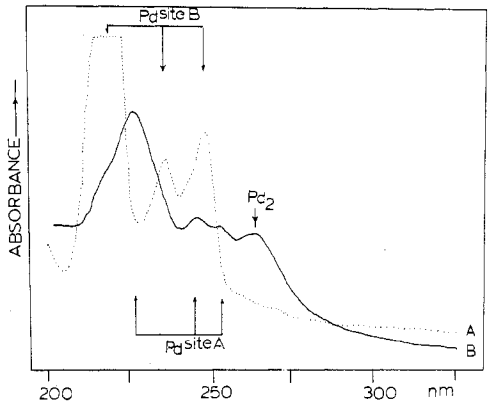


**Figure 9.** Optical spectrum of palladium atoms isolated in solid argon (A) after deposition at 10–12 K and (B) after deposition at 20–25 K, showing the appearance of a new absorption at 265 nm associated with $Pd_2$.

orbital schemes of homonuclear and heteronuclear transition-metal diatomics. Straightforward application of literature VOIP's and orbital exponents with slightly adjusted overlap integrals[22] (Table VII) resulted in the MO scheme shown in Figure 7A. Total energy calculations indicated a shallow minimum at 2.5 Å, with an unreasonably low bond dissociation energy of around 10 kcal/mol. As the d-orbital splitting is usually underestimated by EH methods compared to more sophisticated SCF–X$\alpha$ methods,[21] this result should only be regarded as a first, crude approximation. However, it is noteworthy that with the chosen EH parameters the correlation between observed and calculated optical transitions is satisfactory (Table VII).

**Palladium.** Atomic palladium isolated in a variety of inert-gas matrices has been a source of mystery for quite some time. In brief, the purported matrix spectrum originally published by Mann and Broida[23] was subsequently shown to arise from $Pd(N_2)_{1,2}$ impurities and the authentic atomic palladium spectrum was thus reassigned.[24] Since these early studies, we have conducted further experiments in Ar, Kr, Xe, propane, and hexane matrices. The results obtained conclusively establish that the spectrum of atomic Pd basically consists of a high-energy triplet (200–250 nm) which is surprisingly intense when one considers that two of the transitions are basically of the spin-forbidden type with low gas-phase oscillator strengths.[15] The spectrum of Pd in Kr, for example, consists of a doublet of triplets (Figure 8) where one triplet is observed to completely collapse on annealing at 20 K, indicating the removal of an unstable matrix site concomitant with intensity loss of the other triplet. No unequivocal explanation of this effect can be forwarded at this time, although we note that the phenomenon is far less pronounced in hydrocarbon matrices, pointing to a matrix site effect.

Relatively large, blue, matrix-induced frequency shifts of the order of 2000–5000 cm$^{-1}$ are observed for all lines of atomic Pd (Table VIII). Particularly noteworthy are the exceptionally large, blue shifts of the Pd lines in Xe, resulting in the order of matrix-induced shifts Xe > Kr > Ar > $C_3H_8$ > $C_6H_{14}$, a trend which has been suggested to indicate a substantial, specific metal atom–matrix interaction between the polarizable metal palladium and the most polarizable of the inert gases, xenon.[24]

The ground state of atomic palladium is known to be $d^{10}$. Consequently, one might expect matrix-isolated $Pd_2$, if capable of existence, to be a van der Waals molecule. Indeed, from gas-phase, mass-spectrometric investigations, the dissociation energy of $Pd_2$ has been estimated at 22 ± 10 kcal/mol.[25] The search for the palladium dimer proved to be quite challenging. Pd atom concentration studies in freshly deposited argon and krypton matrices at 10–12 K showed little evidence of any new lines. However, upon annealing of these matrices, a very weak *new* absorption could be observed to grow in at 265 nm in argon (25 K) and 283 nm in krypton (35 K), concomitant with the loss of Pd atom intensity. This new absorption is present in concentrated matrices deposited at 20–25 K (Figure 9, Table VI). Due to the extremely low oscillator strength of this absorption, the metal nuclearity of the associated species could

(22) E. Clementi and J. Roetti, *At. Data Nucl. Data Tables*, **14** (3–4), 445 (1974).
(23) D. M. Mann and H. P. Broida, *J. Chem. Phys.*, **55**, 84 (1971).
(24) W. Klotzbücher and G. A. Ozin, *Inorg. Chem.*, **15**, 292 (1976).
(25) S. S. Lin, B. Strauss, and A. Kant, *J. Chem. Phys.*, **51**, 2282 (1969).

Table IX. Band Assignments and Matrix Shifts for Matrix-Isolated Gold Atoms (Ground State $5d^{10}6s^1$; $^2S_{1/2}$)

| gas | argon | | krypton | | $CH_4$ | | xenon | | cyclohexane | |
|---|---|---|---|---|---|---|---|---|---|---|
| $\nu$, $cm^{-1}$ | $\nu$, $cm^{-1}$ | $\Delta\nu$, $cm^{-1}$ | $\nu$, $cm^{-1}$ | $\Delta\nu$, $cm^{-1}$ | $\nu$, $cm^{-1}$ | $\Delta\nu$, $cm^{-1}$ | $\nu$, $cm^{-1}$ | $\Delta\nu$, $cm^{-1}$ | $\nu$, $cm^{-1}$ | $\Delta\nu$, $cm^{-1}$ |
| 41 174 | 44 345 | −3171 | 43 103 | −1929 | 42 462 | −1288 | 41 067 | 707 | 40 650 | 524 |
| 41 174 | 43 763 | −2589 | 42 553 | −1379 | 41 666 | −492 | 40 567 | 607 | 39 525 | 1649 |
| 37 359 | 39 215 | −1856 | 38 314 | −955 | 37 313 | 46 | 36 832 | 527 | 35 087 | 2272 |

not be unequivocally determined. If one considers (i) that some small activation energy is apparently required in the formation of the species (20–25 K deposition temperature), (ii) that under the dispersions employed the formation of higher clusters seems unlikely, and (iii) that one would expect electronic transitions from a closed, d-shell diatomic to the lowest unoccupied levels composed mainly of 5s/5p orbitals to be weak, then one might reasonably speculate that the new UV absorption is indeed associated with dipalladium, $Pd_2$.

Further support for this assignment stems from EH calculations for $Pd_2$. With use of the parameters listed in Table VIIA, the MO scheme shown in Figure 7 was obtained. With the assumption of a closed-shell configuration, the $Pd_2$ molecule can be seen to be of the van der Waals type. Consequently an electronic transition from the d-orbital manifold to the antibonding $s\sigma_u$ orbital can be expected to be weak, and the lowest observable excitation might therefore be of the $d \rightarrow p\pi$ type, calculated at roughly 38 000 $cm^{-1}$ (263 nm) (Table VII). This is encouragingly close to the experimental result.

**Gold.** The optical spectrum of gold atoms in noble-gas matrices is known to consist of three main absorptions[26] representing transitions from a $^2S_{1/2}$ ground state to a spin–orbit and vibronic split $^2P$ state and has been discussed in depth by Gruen.[26] In our search for the optical spectra of very small gold clusters, we reinvestigated the atomic spectrum. Although our spectra of Au atoms in argon are in excellent agreement with Gruen's data,[26] investigations in Kr, Xe, $CH_4$, and cyclohexane matrices clearly indicated that some high-energy lines above 45 000 $cm^{-1}$, observed by Gruen and associated with atomic gold, were not present in our high-dilution studies and are shown to be part of the spectrum of gold clusters.

It is worth noting the trend in matrix-induced shifts from the gas-phase values (Table IX). While Ar, Kr, and $CH_4$ matrices (the latter often exhibit shifts similar to those in argon) all display *blue* shifts of varying magnitudes, both xenon and especially cyclohexane exhibit *red* shifts of up to 2000 $cm^{-1}$, indicative of the effect of placing gold into substitutional sites of first smaller, equal, and then larger dimensions than those of atomic gold itself.

For further discussion let us concentrate on the spectra of gold species in argon (Figure 10). Irradiation into the 255-nm Au absorption results in the growth of absorptions on the lower energy side of the major atom lines at 223 and 258 nm. These features vanish upon bulk annealing, indicative of a *site photoredistribution process* in which a metal atom in a stable matrix site is transferred to and trapped in a different, unstable matrix site. This effect has also been observed for Ag.[30] During this matrix treatment a new, weak absorption was observed to grow in at 208 nm. In metal concentration studies the new 208-nm line is observed more clearly, accompanied by weaker absorptions at 198, 317, and 365 nm (Figure 10B,C). Upon annealing, the new lines at 198/208, 316, and 365 nm remain essentially unchanged, but two new, weak absorptions are observed to grow in at 292 and 471 nm, accompanied by a slight loss of atomic Au. Irradiation into the

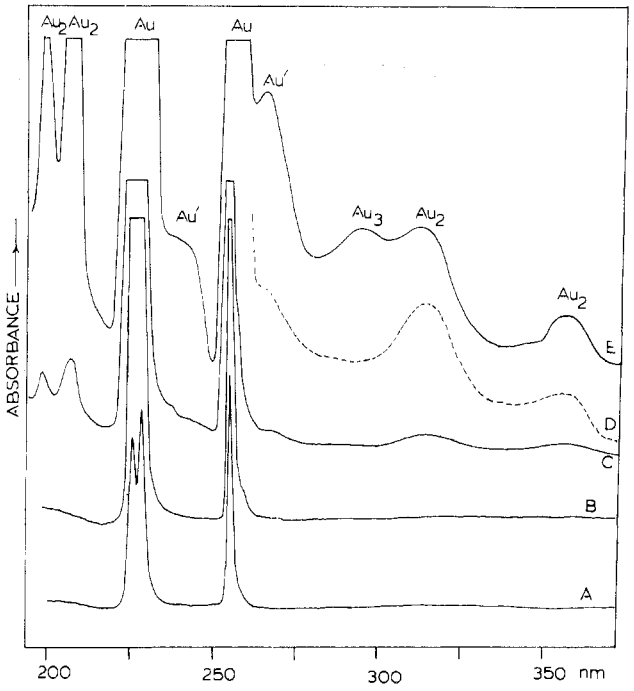


**Figure 10.** Optical spectrum of gold vapor cocondensed with argon: (A) Au/Ar ≃ $1/10^4$, short deposition at 10–12 K; (B) Au/Ar ≃ $1/10^4$, longer deposition at 10–12 K; (C) Au/Ar ≃ $1/10^4$ at 15–20 K; (D) 5 times the expansion of (C); (E) Au/Ar ≃ $1/10^3$ at 15–20 K, showing the growth of $Au_2$ and $Au_3$ clusters and the existence of an unstable trapping site of atomic gold labeled Au′ (see text).

Au atomic resonance line at 255 nm did not have any further effect on these lines.

It was hoped that the formation of these species could be enhanced by raising the matrix deposition temperature, thereby promoting diffusion/aggregation processes in the reaction zone. In a series of deposition temperature studies, the loss of Au atom absorption intensity indicated the presence of Au agglomeration. However, significant growth of the 198/208 nm and associated absorptions was not apparent. Our best results were obtained at 15 K with high metal deposition rates. As the observed gold cluster UV absorptions were too weak to allow meaningful metal concentration studies, any nuclearity assignment has to be tentative at this time. However under the chosen conditions it would seem most plausible to assign the absorptions at 198/208, 317, and 365 nm to the digold species, with those at 292 and 471 nm associated with a higher gold cluster, possibly $Au_3$ (Table VI).

Some insight into the electronic assignments for matrix-isolated $Au_2$ and $Au_3$ can be derived by comparison with the available gas-phase observations of the two-band systems associated with $Au_2$[27,28] and recent relativistic molecular

(26) L. Brewer and G. King, *J. Chem. Phys.*, **53**, 3981 (1976); D. M. Gruen, S. L. Gaudioso, R. L. McBeth, and J. L. Lerner, *ibid.*, **60**, 89 (1974); F. Forstmann, D. M. Kolb, D. Leutloff, and W. Schulze, *ibid.*, **66**, 2806 (1977); D. M. Gruen in "Cryochemistry", M. Moskovits and G. A. Ozin, Eds., Wiley, New York, 1976, p 451, and references therein.

(27) J. Ruamps, *Ann. Phys. (Paris)*, **13**, 1111 (1959).
(28) L. L. Ames and R. F. Barrow, *Trans. Faraday Soc.*, **63**, 39 (1967).
(29) W. E. Klotzbücher, Ph.D. Thesis, "Bimetal Vapour Chemistry", University of Toronto, 1979.
(30) S. Mitchell, J. Farell, G. A. Ozin, and G. Kenney-Wallace, *J. Am. Chem. Soc.*, in press.
(31) D. M. Gruen in "Cryochemistry", M. Moskovits and G. A. Ozin, Eds., Wiley, New York, 1976, Chapter 10.

Table X. Optical Spectra and Electronic Assignments for Disilver, Digold, Trisilver, and Trigold in a Solid Argon Matrix at 10–12 K

| $Ag_2/Ar^{32-34}$ | $Au_2/Ar$ | $Au_2$/gas[27,28] | assignt[a] |
|---|---|---|---|
| | | 500 | A–X |
| 385/406 | | | A–X ($2\sigma_g \rightarrow 2\sigma_u$) |
| | 365 | 380 | B–X |
| | 317 | | ? |
| 261/265 | | | C–X ($2\sigma_g \rightarrow 2\pi_u$) |
| 227 | | | E–X ($1\pi_g \rightarrow 2\sigma_u$) |
| | 198/208 | | ? |

| $Ag_3/Ar^{32-34}$ | $Au_3/Ar$ | assignt[a,b] |
|---|---|---|
| | 471 | ? |
| 440 | | ($2\sigma_u \rightarrow 4\sigma_g$) |
| | 292 | ? |
| 245 | | ($2\sigma_u \rightarrow 2\pi_u$) |

[a] The problems involved with cross correlating assignments between $Ag_{2,3}/Au_{2,3}$ are discussed in the text. [b] Linear geometry favored with a $^2\Sigma_u^+$ electronic ground state.

quantum mechanical calculations for $Au_2$.[35] These can then be compared and contrasted with the electronic assignments for $Ag_2$ and $Ag_3$ derived from gas-phase spectroscopic,[36] matrix optical[32] and MCD spectroscopic,[33] selective cluster cryophotochemical,[32] and SCF–X$\alpha$–SW molecular orbital techniques.[32,34]

From the gas-phase rotational analysis of the A–X (500 nm) and B–X (380 nm) systems of $Au_2$,[27,28] the A and B states have been identified as $^1\Sigma_u^+$, or $0_u^+$ in Hund's case c. It would appear that in our matrix study of $Au_2$, the gas-phase system around 500 nm has not been observed.[27,28] However, the higher energy absorption of matrix-entrapped $Au_2$ at 365 nm can be reasonably correlated with the gas-phase B–X system around 380 nm.[27,28] Regrettably, gas-phase studies of $Au_2$ below 380 nm have not as yet been reported, so it is difficult to propose assignments for the high-energy $Au_2$ bands at 317 and 208/198 nm in solid argon.

From the superficial similarity between the optical spectra of $Au_{2,3}$ and $Ag_{2,3}$ seen in Table X, one is initially tempted to deduce electronic assignments for the gold system simply by cross correlating the data with that for the reasonably well-understood silver system.[32–34,36] However, the danger of adopting this procedure for the embryonic clusters of silver and gold can be appreciated by reference to some very recent ab initio effective core potential calculations for $Au_2$, involving all relativistic effects in the ground and excited states.[35] In brief these calculations show that the electronic architectures of $Ag_2$ and $Au_2$ are likely to be quite different. This relates, in part, to large relativistic contributions encountered for $Au_2$ which have the effect of shortening and strengthening the metal–metal bond, primarily from contraction of the 6s orbitals.[35] Like $Ag_2$, the ground state of $Au_2$ was found to be $^1\Sigma_g^+$ which is predominantly a 6s–6s $\sigma_g$-bonding state but which has low-lying excited states originating from the $5d^96s^2$ configuration.[35] In this respect $Au_2$ differs from $Ag_2$, as the $^2D_{5/2}$ and $^2D_{3/2}$ states are 1.136 and 2.556 eV, respectively, above the ground $^2S$ state compared to the next higher levels $^2P_{1/2}$ and $^2P_{3/2}$ at 4.632 and 5.105 eV, respectively, whereas in silver the corresponding $^2D$ and $^2P$ levels are almost degenerate and the respective spin–orbit splittings are also much less. Thus the $^2D$ valence states of gold are not expected to be strongly perturbed by other low-lying states of the same symmetry, which is in contrast to the situation found for silver.[32–34,36] One is therefore led to believe that the electronic structures of diatomic and triatomic clusters of silver and gold are likely to be quite distinct and assignments for gold clusters deduced by analogy with silver quite unrewarding (Table X).

Clearly, further studies will be required to place the electronic assignments of the observed optical transitions of $Au_2/Au_3/Ar$ on a firm footing.

## Discussion

Apart from Gruen's comprehensive analysis of the matrix spectra of Mo and Au atoms[26] and Kolb's investigations of Cu, Ag, and Au atoms in rare-gas matrices,[26] the optical spectra of transition-metal atoms have not been discussed in much detail, either because the experimental data were not available or because pronounced overlap of a multitude of lines prevented a meaningful analysis of the data for isolated atoms.

With this report we have completed an experimental examination[29] of the optical spectra of all transition-metal atoms with the exception of Y, La, Tc, and Os, metals which all require special evaporation methods. It is not the intention of the present study to expand on the theoretical aspects of the interaction between matrix-isolated transition-metal atoms and their surrounding matrix cages. This subject has been reviewed recently.[31] Rather, it seems sufficient here to simply state that, for all metal atoms studied, matrix-induced shifts were of the order of 10% of the respective gas-phase transition energies, indicating the extent of the matrix-cage influence on the different electronic states of the isolated atom. Generally it was found that noble-gas-induced frequency shifts from the gas-phase values were toward higher energies and that the magnitude of the effect depended on the matrix material and the atomic level under consideration. A more detailed picture of excited and ground-state metal atom–matrix cage interactions is expected to emerge from fluorescence studies presently under way in our group.[30]

It is probably fair to state that until the mid-1970s the generation and cryogenic trapping of transition-metal clusters had been accidental and sometimes led to erroneous assignments of atomic species. In fact, the interference of metal atom aggregation effects was considered to be a nuisance in the matrix synthesis of novel mononuclear reactive intermediates and occasionally resulted in incorrect species identification. An example of this problem has been illustrated in the present report, where some digold absorptions were originally mistaken for atomic gold transitions.

We have also partially succeeded in a first systematic attempt to obtain the optical spectra of a wide range of transition-metal homonuclear and heteronuclear diatomic and higher clusters.[29] The spectra of $Zr_2$, $Pd_2$, $Au_2$, and $Au_3$ represent that part of the study which has been plagued by inherent experimental problems and consequently resulted only in tentative cluster assignments.

Nevertheless, these preliminary data should provide valuable information for checking the purity level of metals employed in metal-vapor-matrix synthesis and the degree of atomic isolation achieved in matrix experiments as well as the assessment and further improvement of EH and other more sophisticated molecular orbital calculations for small, well-defined, naked transition-metal clusters.

(32) G. A. Ozin and H. Huber, *Inorg. Chem.*, **17**, 155 (1978); G. A. Ozin and S. A. Mitchell, *J. Am. Chem. Soc.*, **100**, 6776 (1978); G. A. Ozin, H. Huber, D. McIntosh, S. Mitchell, J. G. Norman, Jr., and L. Noodleman, *ibid.*, **101**, 3504 (1979); G. A. Ozin, H. Huber, and S. Mitchell, *Inorg. Chem.*, **18**, 2932 (1979), and references cited therein.

(33) R. Grinter, S. Armstrong, U. A. Jayasooriya, J. McCombie, D. Norris, and J. P. Springall, *Symp. Faraday Soc.*, **No. 14**, paper no. 4 (1980).

(34) G. A. Ozin, D. McIntosh, S. Mitchell, and R. P. Messmer, in preparation; G. A. Ozin, *Symp. Faraday Soc.*, **No. 14**, 1 (1980).

(35) Y. S. Lee, W. C. Ermler, and K. S. Pitzer, *J. Chem. Phys.*, **70**, 293 (1979); Y. S. Lee, W. C. Ermler, K. S. Pitzer, and A. D. McClean, *ibid.*, **70**, 288 (1979).

(36) B. Klemen and S. Lindkvist, *Ark. Fys.*, **8**, 333 (1954); **9**, 385 (1955); J. Ruamps, *Ann. Phys. (Paris)*, **4**, 1111 (1959); R. C. Maheshwari, *Indian J. Phys.*, **31**, 368 (1963); N. Aslund, R. F. Barrow, W. G. Richards, and D. N. Travis, *Ark. Fys.*, **30**, 171 (1965); B. Rosen, "Spectroscopic Data Relative to Diatomic Molecules", Pergamon Press, Elmsford, N.Y., 1970; C. M. Brown and M. L. Ginter, *J. Mol. Spectrosc.*, **69**, 25 (1978).

**Acknowledgment.** We gratefully acknowledge the financial assistance of the National Research Council of Canada's Operating, New Ideas and Strategic Energy programs, Imperial Oil of Canada, Erindale College, and Lash Miller Chemical Laboratories for support of this research.

**Registry No.** Hf, 7440-58-6; W, 7440-33-7; Re, 7440-15-5; Ru, 7440-18-8; Zr, 7440-67-7; Pd, 7440-05-3; Au, 7440-57-5; $Zr_2$, 12597-66-9; $Pd_2$, 12596-93-9; $Au_2$, 12187-09-6; $Au_3$, 75024-07-6.

Contribution from Lash Miller Chemical Laboratories and Erindale College, University of Toronto, Toronto, Ontario, Canada M5S 1A1

# Very Small Bimetallic Clusters of Silver with Manganese, Molybdenum, and Copper in Rare Gas Matrices

W. E. KLOTZBÜCHER and G. A. OZIN*

*Received December 28, 1979*

The simultaneous codeposition of silver vapor with manganese, molybdenum, and copper vapor in low-temperature argon matrices at 10–12 K provides a synthetic pathway to low-nuclearity, bimetallic clusters, some of which are of the low-miscibility class in the respective binary alloy systems. Mixed-metal concentration, annealing, and selective photoaggregation studies in combination with optical absorption spectroscopy allow the tentative identification of AgMn, AgMo, and AgCu molecules as well as some less well-defined, higher bimetallic clusters. A preliminary view of the electronic and bonding architecture of these bimetallic combinations is obtained from extended Hückel calculations, and some comments are forwarded on the relevance of these studies to concepts in the field of alloy and bimetallic cluster catalysis.

## Introduction

The interactive electronic architecture which has recently emerged from the very low-nuclearity cluster systems $Cr_nMo_m$[1] and $Cr_nAg_m$[2] entrapped within weakly interacting, low-temperature supports has provided an interesting new perspective with which to view highly dispersed, multimetallic cluster catalysts comprised of partially immiscible or wholly immiscible components.[3] In contradistinction, the striking, noninteractive characteristics observed at the atomic level for the Pd/Ag and Pd/Mo[4] combinations alert one to the fact that the simple mixing of metal atomic vapors under cryogenic conditions is not sufficient to ensure reactive encounters and the formation of bimetallic clusters. Clearly, more subtle factors of an electronic and kinetic nature can contribute to and markedly affect the early stages of bimetallic cluster growth at low temperatures, even though the respective bulk-phase diagrams may imply total miscibility of the metallic components over the entire concentration range.[5]

For determination of the generality of the above observations and the scope of the method for synthesizing controlled-size, multimetallic clusters for spectroscopic, theoretical, and chemical investigations, a systematic study of a wide range of metallic combinations needs to be undertaken. The basic requirements for progress in this area are, first, fairly well-understood parent cluster systems and, second, minimal spectral interference of atomic and cluster species in the two-component systems. In this context, the small cluster systems $Cu_{2,3}$,[6] $Ag_{2,3}$[6b,7] and $Mo_{2,3}$[1,8] are reasonably well suited for bimetallic undertakings.

Following up on some earlier matrix work which suggested anomalously facile aggregation pathways in the Mn/CO system[9] (e.g., Mn/CO $\simeq$ 1/10[3] yields almost exclusively $Mn_2(CO)_{10}$ at 10–12 K), it was thought worthwhile to elucidate the aggregation characteristics of Mn in rare gas matrices (thereby completing the cluster studies of the first transition series[10]) with an extension to bimetallic combinations. The results obtained with the metallic pairs Ag/Mn, Ag/Mo, and Ag/Cu will be described in this paper, the unifying theme being the presence of silver in all three systems investigated.

## Experimental Section

Our experimental setup for metal and bimetal vapor depositions has been described previously.[1] Monoatomic metal vapors were generated by direct resistive heating (ac) of either a metal filament (Mo), a tungsten support (Cu), or a tantalum Knudsen cell (Ag, Mn) suspended between two water-cooled electrodes. Tungsten supports and tantalum Knudsen cells were manufactured in the University of Toronto workshops without the use of oil-based solvents and were thoroughly outgassed in vacuo before use. (Manganese evaporation from graphite Knudsen cells treated identically showed similar results.) The metals were of better than 99.99% purity, with the metal flow quantitatively and continuously monitored by a dual quartz-crystal microbalance assembly. The matrix gas flow was controlled by a calibrated micrometer needle valve and thermocouple vacuum gauge assembly. A Displex closed-cycle helium refrigerator was used to cool a NaCl optical window to 10–12 K, the temperature being monitored by a Au–0.07 atom % Fe thermocouple embedded in a drilled cavity

(1) W. E. Klotzbücher and G. A. Ozin, *J. Am. Chem. Soc.* **100**, 2262 (1978); *J. Mol. Catal.*, **3**, 195 (1977); W. E. Klotzbücher, G. A. Ozin, J. G. Norman, Jr., and H. J. Kolari, *Inorg. Chem.*, **16**, 3871 (1977).
(2) W. E. Klotzbücher and G. A. Ozin, *Inorg. Chem.*, **18**, 2101 (1979).
(3) J. H. Sinfelt and J. A. Cusumano in "Advanced Materials in Catalysis", J. J. Burton and R. L. Garten, Eds., Academic Press, New York, 1977; J. H. Sinfelt, *Acc. Chem. Res.*, **10**, 15 (1977), and references cited therein.
(4) W. E. Klotzbücher and G. A. Ozin "Photoselective Bimetallic Aggregation", Proceedings of the NBS Conference on High Temperature Science, Washington, D.C., 1978.
(5) M. Hansen, "Constitution of Binary Alloys", McGraw-Hill, New York, 1958, and supplements.
(6) (a) M. Moskovits and J. Hulse, *J. Chem. Phys*, **67**, 4271 (1977); (b) G. A. Ozin, H. Huber, D. McIntosh, S. Mitchell, J. G. Norman, Jr., and L. Noodelman, *J. Am. Chem. Soc.* **101**, 3504 (1979).
(7) H. Huber and G. A. Ozin, *Inorg. Chem.*, **17**, 155 (1978); G. A. Ozin and S. Mitchell, *J. Am. Chem. Soc.*, **100**, 6776 (1978); *Inorg. Chem.*, **18**, 2932 (1979); W. Schulze, H. U. Becker, and H. Abe, *Chem. Phys.*, **35**, 177 (1978); T. Welker and P. T. Martin, *J. Chem. Phys.*, **70**, 5683 (1979); D. M. Gruen and J. K. Bates, *Inorg. Chem.*, **16**, 2450 (1977).
(8) W. E. Klotzbücher and G. A. Ozin, *Inorg. Chem.*, **16**, 984 (1977).
(9) G. A. Ozin, H. Huber, E. P. Kündig, and A. J. Poë, *J. Am. Chem. Soc.*, **97**, 308 (1975).
(10) W. E. Klotzbücher, Ph.D. Thesis, "Bimetal Vapour Chemistry", University of Toronto, 1979.

0020-1669/80/1319-3776$01.00/0 